Regional Changes in the Interannual Variability of U.S. Warm Season Precipitation

SCOTT J. WEAVER

NOAA/Climate Prediction Center, College Park, Maryland, and Environmental Defense Fund, Washington, D.C.

STEPHEN BAXTER AND KIRSTIN HARNOS

NOAA/Climate Prediction Center, College Park, Maryland

(Manuscript received 25 November 2014, in final form 5 April 2016)

ABSTRACT

Intensification of regional springtime precipitation variability over the United States and the role of North American low-level jets (NALLJs) are investigated for the 1950–2010 period. The analysis reveals that the primary modes of NALLJ fluctuations are related to the strengthening of AMJ precipitation variability over the northern Great Plains and southeastern United States during the last 60 years. Examination of the epochal change in NALLJ variations shows a stronger connectivity to SST variability during 1980–2010 than in the 1950–79 period. In the context of the first three NALLJ variability modes it appears that the role of decadal SST variations (NALLJ mode 1) and the recent emergence of tropical Pacific connectivity (NALLJ modes 1 and 2) via SST-induced atmospheric heating and large-scale circulation changes may act to strengthen and spatially shift the NALLJ variability modes southward and/or eastward, intensifying regional precipitation variability in the recent epoch. Although notable NALLJ variability also exists in the earlier epoch, the upper-level height field is significantly lacking in meridional gradients, leading to weak upper-level zonal wind anomalies over the United States and diminished NALLJ variability. Conversely, the intensified and spatially shifted upper-level height anomaly in the recent epoch produces enhanced meridional height gradients in all three modes, strengthening NALLJ variability—highlighting that seemingly subtle shifts in hemispheric-scale atmospheric circulation changes can have important impacts on regional climate variability and change.

1. Introduction

The demand for regional climate information is increasing within the national and international climate science and user communities. An important aspect of this need is an enhanced understanding of the physical mechanisms that produce regional precipitation variability and whether this variability has changed. This question is important for efforts to clarify the future trajectory of regional climate variability and change and is paramount for climate mitigation and adaptation strategies, as enhanced understanding of these characteristics will lead to improved predictions and projections of the magnitude of regional manifestations of warm season drought, pluvial, and severe weather.

During the spring and summer large amounts of heat and moisture are transported northward into the central and eastern United States by the low-level atmospheric circulation. Figure 1 highlights this feature and shows the mean meridional 850-hPa wind and mean precipitation (Fig. 1, top) for April–June (AMJ) over 1950–2010. While the climatological Great Plains low-level jet (GPLLJ) is clearly evident by the strong wind maxima over central Texas, the mean flow also extends eastward to the southeast coast of the United States, encompassing much of the eastern two-thirds of the nation. Although the GPLLJ is the most well-known feature of the warm season circulation over the United States, and is the primary mechanism for warm season Great Plains precipitation, anomalous jetlike excursions to areas outside of the Great Plains are

Corresponding author address: Dr. Scott J. Weaver, Environmental Defense Fund, 1875 Connecticut Ave. NW, Washington, DC 20009.
E-mail: sweaver@edf.org

DOI: 10.1175/JCLI-D-14-00803.1

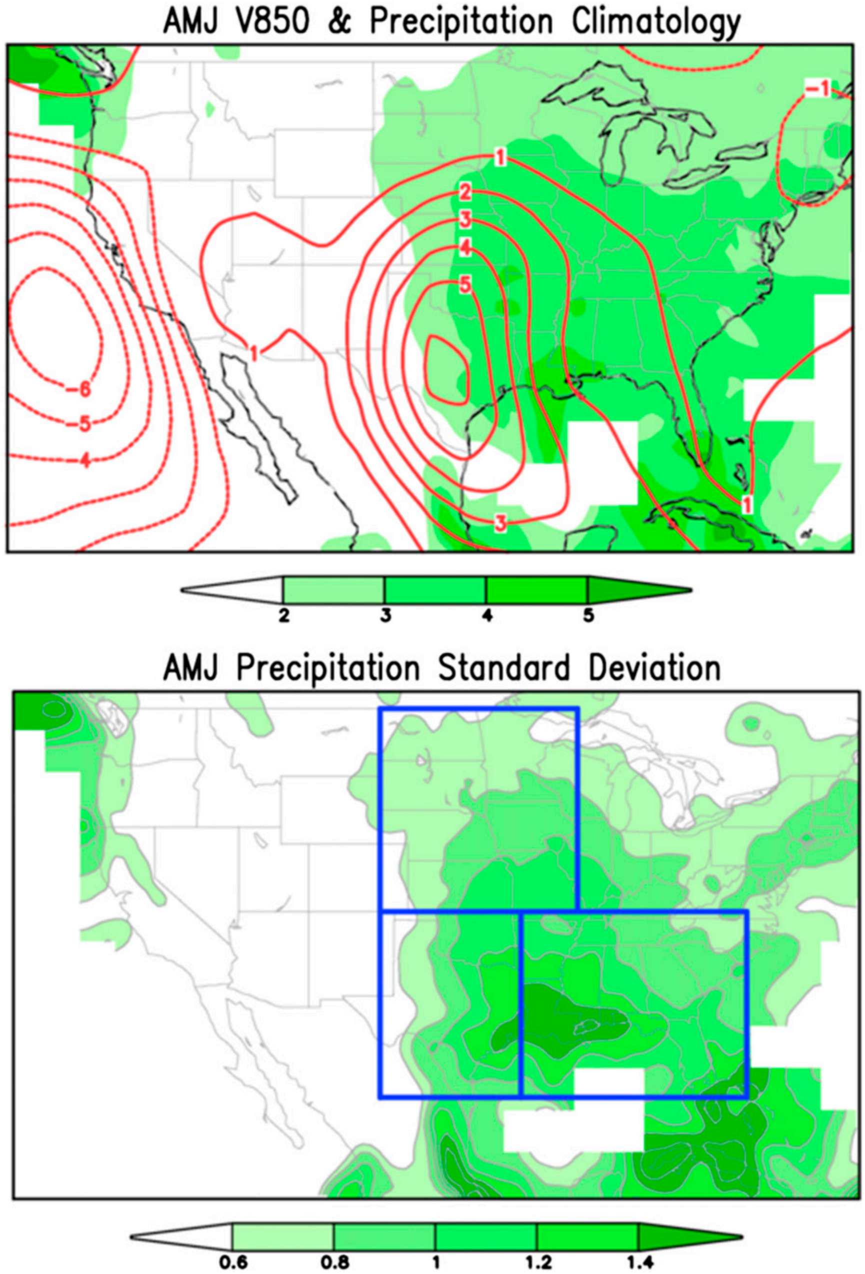

FIG. 1. (top) Warm season climatology of precipitation (shaded) and the 850-hPa meridional winds (contoured) for 1950–2010. Wind anomalies >1 m s^{-1} are contoured at 1 m s^{-1} intervals and precipitation >2 mm day^{-1} is shaded. The positive (negative) contours denote southerly (northerly) meridional wind components. (bottom) The standard deviation of AMJ precipitation for the period 1950–2010. Precipitation standard deviation >0.6 mm day^{-1} is shaded and contoured at 0.2 mm day^{-1} intervals. The blue-outlined boxes are referenced in Fig. 2.

commonplace [hence the term North American low-level jet (NALLJ)] and have recently been recognized for their significant impact on extreme precipitation events, drought, severe weather, and temperature trends (Ruiz-Barradas and Nigam 2005; Weaver et al. 2009, 2012; Weaver 2013).

In addition to clarifying the regional impacts of NALLJ variability on the subcontinental scale, recent efforts have uncovered NALLJ links to the large-scale climate variability, highlighted by the connection between global-scale SST variability and NALLJ fluctuations (Weaver et al. 2009), including their springtime

(AMJ) epochal changes (Weaver et al. 2012 and Fig. 6 herein). Given that NALLJs are vitally important for communicating the large-scale climate influences to regional impacts, the link to climate boundary forcing (i.e., global SST), its epochal changes, and how this SST variability is related to large-scale atmospheric circulation anomalies in which NALLJ variability is embedded is analyzed here. This is fundamental to understanding how the large-scale remote climate influences are manifested in the context of regional climate variability.

Changes in U.S. warm season regional climate variability are already being observed. Recent studies suggest that during meteorological summer (JJA) the interannual variability of precipitation over the southeastern United States has intensified over the last six decades (Wang et al. 2009; Wang et al. 2010; Li et al. 2011). These changes are potentially the result of southward shifts in upper-level atmospheric zonal jet stream activity (Wang et al. 2010) and westward expansion of the North Atlantic subtropical high (NASH)—two influences that have also been shown to be related to NALLJ variations (Weaver and Nigam 2008; Weaver et al. 2009). Additionally, springtime tornadic activity has also undergone changes in variability; however, the exact cause remains elusive (Brooks et al. 2014).

Given the role of NALLJs in generating spring season precipitation variability and tornadic activity over the U.S. Great Plains and southeastern United States, and their linkage to global-scale SST and large-scale atmospheric circulation variations, questions arise as to whether these regions have similarly experienced intensification of springtime precipitation variability and the role of NALLJs in these changes. As such, the goal here is to employ an atmospheric circulation–centric analysis strategy, focusing on the role of NALLJ variability in changes to springtime interannual variability of precipitation over the Great Plains and southeastern United States.

2. Data and methodology

NALLJ variability for the 1950–2010 period is assessed by conducting an empirical orthogonal function (EOF) analysis on the seasonal anomalies of 850-hPa meridional wind field over the domain 20°–50°N, 105°–80°W in the NCEP–NCAR reanalysis (Kalnay et al. 1996). As in Weaver et al. (2012) a covariance-based analysis on the latitudinally weighted field was performed. The EOFs are not rotated given the limited analysis domain. The principal components (PCs) obtained from this analysis are used as indices in relating NALLJ variability to large-scale climate features (i.e., SST, 200-hPa geopotential height, and 200-hPa zonal wind) and seasonal precipitation anomalies through correlation analysis and calculation of 30-yr moving standard deviation time series. The epochal comparisons are conducted by restricting the PC time series to the 1950–79 and 1980–2010 periods, and performing regressions to 850-hPa meridional wind and precipitation, as opposed to calculating the EOF loading patterns for each period separately—highlighting the epochal changes to the full 61-yr NALLJ modes. The rainfall data are from the Precipitation Reconstruction (PREC) (Chen et al. 2002) updated by the NOAA/Climate Prediction Center (CPC) (http://www.cpc.ncep.noaa.gov/products/precip/realtime/GIS/USMEX/analysis.shtml). We also employ the use of observed outgoing longwave radiation (OLR) data from the NOAA Advanced Very High Resolution Radiometer (AVHRR; Liebmann and Smith 1996). SST linkages are facilitated by using the Extended Reconstructed SST, version 3 (ERSST.v3) (Smith et al. 2008). NALLJ reconstructed precipitation anomalies are formed by taking the product of the precipitation regression pattern for each of the first three modes of NALLJ variability and the PC value for each year to make a reconstructed precipitation time series for each mode, then summing those contributions to form the NALLJ modes 1–3 reconstructed precipitation anomaly time series.

As in Weaver and Nigam (2008) we employ the Rossby wave source (RWS) to analyze the potential for large-scale atmospheric circulation links to tropical forcing. The RWS contains terms involving divergent flow:$\mathrm{RWS} = -\nabla \cdot (\mathbf{v}'_\chi \zeta_c) - \nabla \cdot (\mathbf{v}_{\chi,c} \zeta')$, where $\mathbf{v}_\chi$ is the divergent component of the wind, ζ is the absolute vorticity ($\eta + f$), and primes and subscript c denote anomaly and climatology, respectively. The first term on the rhs is generally dominant and can be expressed as the sum of a tropical ($-\mathbf{v}'_\chi \cdot \nabla \zeta_c$) and extratropical ($-\zeta_c \nabla \cdot \mathbf{v}'_\chi$) RWS component. Given the meridional reach of tropical divergent outflows ($\mathbf{v}'_\chi$), the RWS can be large thousands of kilometers northward of an equatorial diabatic heating anomaly, especially in the western Pacific sector, where meridional vorticity gradients ($\nabla \zeta_c$) are large in the extratropics due to the presence of the Asian-Pacific jet.

3. Precipitation variability

a. Spatial variations

The AMJ precipitation variability (Fig. 1, bottom) has similar characteristics to the mean precipitation (i.e., decreasing magnitude to the north and west) with a maxima along the Gulf Coast, and exhibits substantial variability over much of the eastern two-thirds of the nation. Using the geographical placement of the mean meridional wind and spatial standard

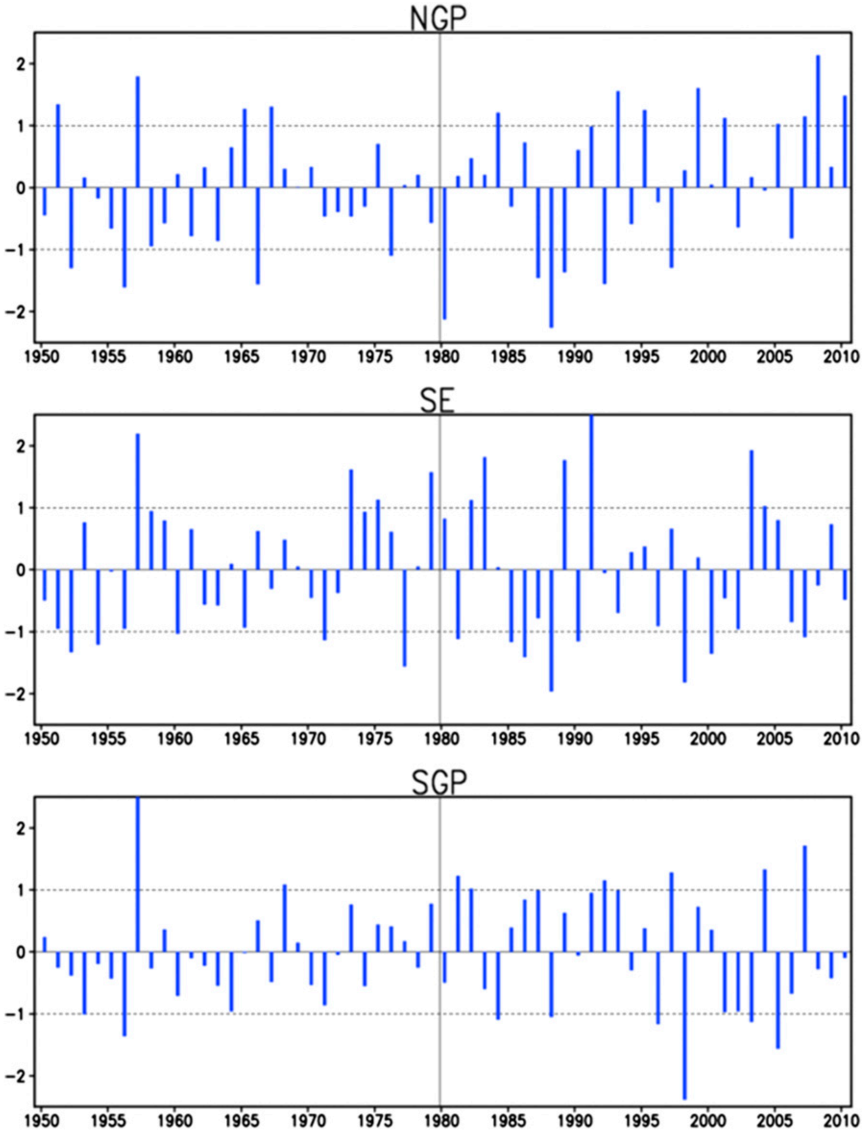

FIG. 2. Normalized time series of AMJ precipitation anomaly indices for 1950–2010 for the (top) NGP, (middle) SE, and (bottom) SGP regions. Area averaging is conducted within the latitude and longitude regions shown in Fig. 1 and values are expressed in units of standard deviation.

deviation of precipitation as a guide, three key areas may be defined for regional precipitation variability analyses, as outlined by the boxed regions in the bottom panel of Fig. 1. The areas comprise the northern Great Plains (NGP; 37°–49°N, 104°–90°W), southern Great Plains (SGP; 26°–37°N, 104°–94°W), and southeastern United States (SE; 26°–37°N, 94°–78°W). Furthermore, all three of these regions are prone to recurrent droughts, pluvials, and severe weather over the last 65 years, highlighted most recently by the NGP (SGP) flooding in 2008 (2015), the multiyear drought over the SGP during 2011–14, and the major SE tornado outbreaks and flooding in spring 2011.

b. Evolution of temporal variability

To understand the changes in springtime regional precipitation variability it is necessary to examine the time series evolution of precipitation anomalies during the spring. Figure 2 shows the AMJ standardized anomalies of precipitation from 1950–2010 over the NGP (top panel), SE (middle panel), and SGP (bottom panel). Splitting the time series into early (1950–79) and recent (1980–2010) epochs (as in Wang et al. 2010) shows that the interannual variability of AMJ precipitation has increased markedly in all 3 regions, with precipitation anomalies exceeding one standard deviation increasing from 8 to 14 over the NGP, from 9 to 14 over the SE, and from 4 to 12 over the SGP. Also noteworthy is that in the early period there are only two instances accumulated across all regions with a seasonal precipitation anomaly exceeding two standard deviations, while in the recent period that increases to five cases, and includes one instance in the SE region where precipitation exceeded three standard deviations during AMJ of 1991. Statistical significance of the changes in regional precipitation variability were assessed by conducting the Brown–Forsythe test, with all regions passing at the 95% level.

To help identify the impact of individual outliers and capture the temporal evolution of the variability changes, Fig. 3 shows a moving centered 30-yr standard deviation of precipitation (solid lines) and its linear trend (dashed lines) for the NGP (top panel), SE (middle panel), and SGP (bottom panel) beginning in 1950.[1] The 30-yr moving standard deviation of precipitation increases in all regions during AMJ (as does its linear trend line), consistent with the similarly noted increases in interannual variability as a function of epoch in the time series displayed in Fig. 2. To be sure, there are fluctuations around the trend line, which is not surprising given the potential for outliers to impact the 30-yr moving standard deviations. For instance, the early period spike over the SGP is likely due to the strong anomaly that occurred during the spring of 1957 (Fig. 2). Had this excessively strong anomaly not occurred, the trajectory of the precipitation variability would have a weaker standard deviation over the SGP during the early portion of the record, leading to an even stronger positive trend in its variability.

Attributes such as these highlight the importance of conceptualizing variability changes in the context of both the evolution of precipitation variability, as captured in the moving standard deviations, and their epochal changes. Solely relying on either moving standard deviation or epochal changes may potentially lead to undue conclusions regarding the characteristic change to the variability, because the moving standard deviation is sensitive to outliers, while the one standard deviation threshold count used in the epochal stratification have the potential to understate or overstate changes in variability.

4. NALLJ variability

a. Recurrent variability modes

Instrumental to warm season regional climate variability are NALLJ fluctuations, which play a critical role in generating and focusing regional patterns of precipitation variability during the spring and summer months (Higgins et al. 1997; Schubert et al. 1998; Weaver and Nigam 2008). Shown in Fig. 4 (similar to Fig. 2 from Weaver et al. 2012) are the regressions of meridional wind (contours) and precipitation (shaded) against the time series of the first three modes of AMJ NALLJ variability for 1950–2010 (left panels), 1950–79 (center panels), and 1980–2010 (right panels), highlighting the epochal changes as diagnosed from the NCEP–NCAR reanalysis (Kalnay et al. 1996).[2] Recall that the epochal comparisons are facilitated by subsetting the PC time series by epoch after conducting the EOF analysis on the full 61-yr record. The regression of the meridional wind onto the EOF's for the full 1950–2010 time period will by definition produce the spatial structure of the EOF modes themselves. Together the first three modes explain ~72% of the AMJ regional 850-hPa meridional wind variance with mode 1, mode 2, and mode 3 explaining 41%, 20%, and 11% of the 1950–2010 variance, respectively, and highlight wind and precipitation enhancement and spatial shifting.[3]

All three modes play a critical role in the occurrence of major U.S drought, pluvial, and severe weather episodes, including the Great Plains droughts (pluvial) of 1980 and 1988 (1993), the SE drought of 2006/07, and the record-breaking tornadic activity over the SE in spring 2011. The fraction of precipitation variability explained by the three leading EOF modes varies from 10% to >80% over the 1950–2010 period depending on region and epoch (not shown). Additionally, all three modes and their precipitation impacts have undergone epochal changes, characterized by the positive lobes of modes 1 and 2 shifting south and the negative lobe of mode 3 shifting east during the recent epoch. These shifts may appear trivial upon first glance (i.e., when viewed from a hemispheric large-scale climate perspective); however, they are quite relevant in the context of regional hydroclimate variability and change. Indeed, a comparison of the epochal precipitation changes (center and right panels of Fig. 4) shows an expansion and strengthening of mode 1 and 2 precipitation anomalies, and for mode 3 an erosion of the western edge of the positive precipitation anomaly over the southern tier of the United States and the

[1] For instance, the value plotted for "1965" is actually the standard deviation for 1950–79, the value plotted for "1966" is the standard deviation for 1951–80, and so on.

[2] NALLJ variability was also assessed in NARR and the ERA-40 reanalyses and the patterns were found to be consistent among the reanalysis systems, attesting to the stability of the modes across multiple datasets (Weaver and Nigam 2008).

[3] The NALLJ modes and their precipitation impacts are displayed here in the context of enhancement of moisture and rainfall generation, but they can also be considered in the opposing phase (i.e., in the context of rainfall suppression).

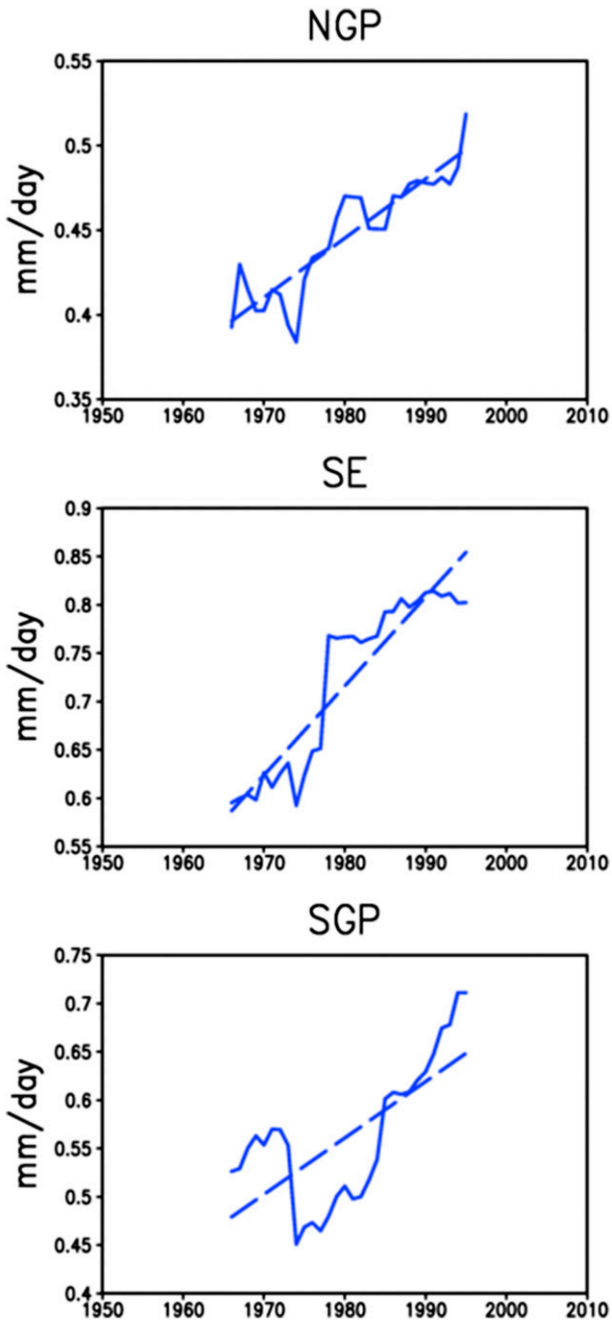

FIG. 3. The 30-yr moving standard deviation of AMJ regional precipitation indices (mm day^{-1}) for the (top) NGP, (middle) SE, and (bottom) SGP regions.

development of negative precipitation anomalies extending from the SGP to the upper Midwest and Ohio River valley regions. Local significance testing of the 850-hPa meridional wind and precipitation regression patterns, and their epochal changes, were assessed using a *t* test, with all major correlation areas passing at the 95% level. Additionally, field significance was tested using the Livezey and Chen (1983) Monte Carlo method. Both the 850-hPa meridional wind and precipitation were found to be field significant at the 95% level.

b. Evolution of reconstructed precipitation

A similar accounting of the time series of NALLJ modes reveals only minor similarities across the two epochs (1950–79 and 1980–2010) when compared to changes in precipitation variability [see Fig. 5 in Weaver et al. (2012) for PC time series]. Among these are slight increases in the instances where the PC1 and PC2 time series exceeds one standard deviation (not shown). The PC3 time series has exactly the same number of extremes in AMJ for the early and recent epochs (10) (not shown). Nevertheless, it is not necessarily expected that an individual NALLJ PC would have similar increases and/or decreases as the regional precipitation indices in the occurrence of seasons exceeding one standard deviation, because each individual NALLJ mode contributes only a portion of the total precipitation variability in a given region, and because it appears that the epochal geographic shift may have as much (if not more) influence on precipitation as does the PC magnitude.

Despite the modest changes from one period to another in the extreme values (i.e., greater than one standard deviation) of the individual NALLJ PCs (not shown), an inspection of the 30-yr moving standard deviation of the reconstructed precipitation anomaly time series from NALLJ modes 1–3 (Fig. 5) reveals some similarities to its total precipitation variability counterpart in terms of the temporal evolution and linear trends of reconstructed precipitation variability. In particular, all NALLJ-reconstructed 30-yr moving standard deviation precipitation time series show an increase, albeit with varying degrees of intensity. The NGP and SE show a stronger association between the total precipitation variability changes and the NALLJ reconstruction, especially over the SE. The NGP-reconstructed variability change is weaker than the total with apparent decadal shifts in variability, as opposed to a more consistent increase, which is not surprising given that this mode has been shown to temporally evolve on multidecadal time scales (Weaver et al. 2012).

The reconstructed variability change over the SGP, while positive, is extremely small compared with the total precipitation variability changes (Fig. 3), indicating the lack of a role for the first three modes of NALLJ fluctuations in contributing to the increasing precipitation variability over that region. This is consistent with the AMJ NALLJ mode 1 and 2 regressions, which show little influence on precipitation anomalies

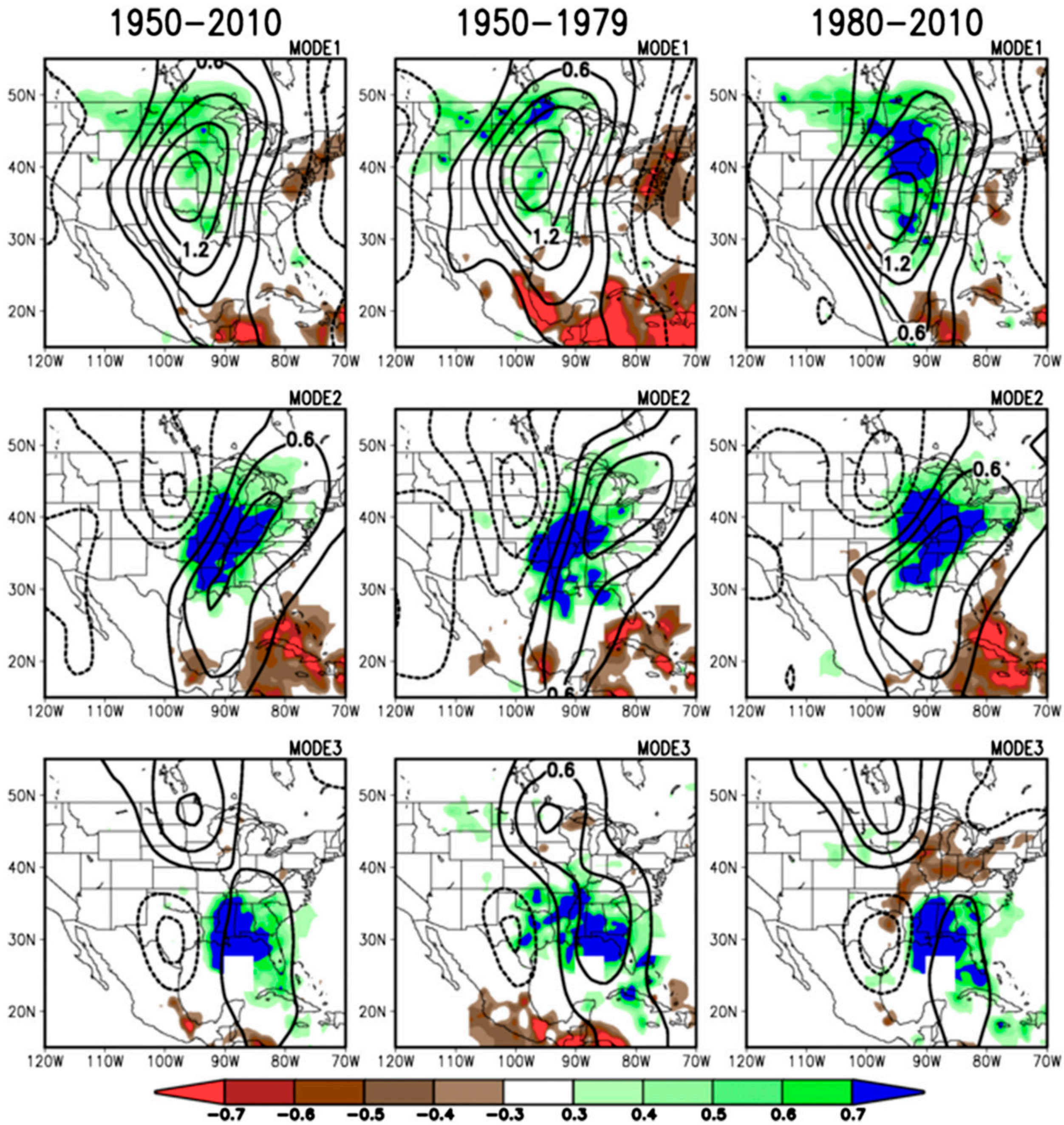

FIG. 4. Recurrent patterns of AMJ NALLJ variability (contours) and precipitation regressions (shaded) for (left) 1950–2010, (center) 1950–79, and (right) 1980–2010 and (top)–(bottom) for modes 1, 2, and 3. The EOF modes are contoured at 0.2 m s^{-1} and precipitation regressions are shaded at 0.1 mm day^{-1} intervals. The epochal comparisons are facilitated by subsetting the PC time series by epoch after conducting the EOF analysis on the full 61-yr record.

over the SGP (Fig. 4). The origin for the large increase in SGP precipitation variability evidently resides in other mechanisms, either lower NALLJ modes or perhaps land–atmosphere interactions and the related interannual variability in land–atmosphere coupling strength (Guo and Dirmeyer 2013).

5. Large-scale climate variability

a. Sea surface temperature

It is important to assess the role of large-scale climate boundary conditions such as sea surface temperature (SST) in the changes in NALLJ-related precipitation

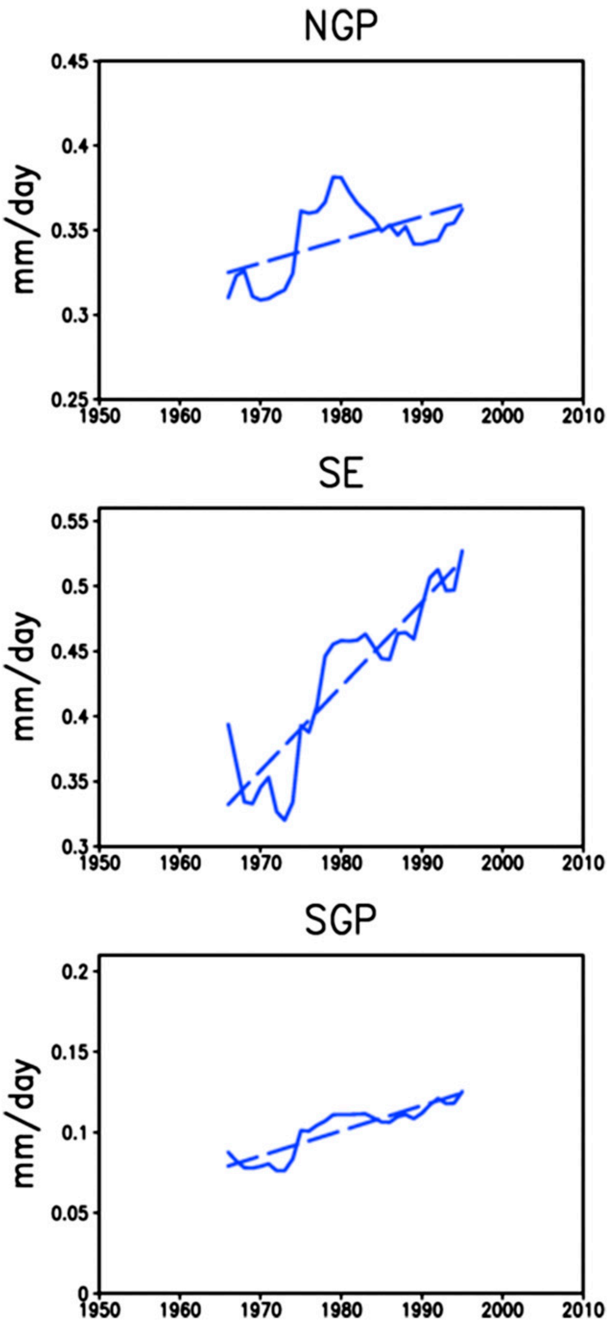

FIG. 5. As in Fig. 3, but for AMJ NALLJ reconstructed precipitation indices.

variability. The link is fundamental to understanding variability changes given the important role that SST variations have in the climate system, and may provide insight into the operative mechanisms. To be sure, the link between the NALLJ and SST has been previously documented over 1950–2010 (Weaver et al. 2009, 2012), although NALLJ mode 3 was not included in those analyses.

Figure 6 shows the correlations between NALLJ PCs and detrended global SST variability as a function of epoch. The contoured areas indicate that the correlation difference from one epoch to another is statistically significant at the 70% (solid) and 90% (dashed) levels as the result of applying randomized sampling 1000 times to the 61-yr record and taking the difference in correlations among these randomized samples for the first 30 and last 31 years of data.

The epochal changes reveal a notable decadal shift in NALLJ mode 1 SST correlations highlighted by a lack of a tropical SST component, but with stronger correlations to the global SST footprints of the Atlantic multidecadal oscillation (AMO) and Pacific decadal oscillation (PDO) for the early and recent epochs, respectively. For NALLJ mode 2 the recent epoch shows the emergence of stronger SST correlations over the tropical Pacific highlighted by an east–west SST gradient (i.e., trans-Niño like), where in the previous epoch there was none. For NALLJ mode 3, there is a warm eastern Pacific (i.e., El Niño like) with much stronger AMJ correlations in the recent epoch when compared to the earlier one.

The importance of NALLJ mode 1 shifts during the recent epoch notwithstanding, analyzing the evolution of tropical Pacific SST linkages to the more strongly interannually varying NALLJ modes 2 and 3 [see Fig. 5 in Weaver et al. (2012) for temporal variability of the PC2 and PC3 time series] during the recent epoch is targeted here given the focus on understanding recent changes to the interannual variation in precipitation.[4] It is further necessary to assess the SST connectivity in the context of the evolving state of the tropical Pacific, as opposed to only contemporaneously, given that recent studies indicate a significant role for ENSO decay and/or emergence in springtime precipitation variability over the United States (Lee et al. 2014).

Shown in Figs. 7 and 8 are the five-season lag–lead regressions (from −3 to +1 seasons) of the 1980–2010 AMJ PC time series for NALLJ modes 2 (Fig. 7) and 3 (Fig. 8), respectively. The evolution of the negative SST anomalies for NALLJ mode 2 are focused primarily over the central tropical Pacific with the strongest regressions occurring during the preceding fall and winter, and a precipitous decay in the central Pacific from January–March (JFM) to AMJ, culminating in the development of a warm far eastern Pacific contemporaneous SST structure during AMJ, which continues into July–September (JAS), and is reminiscent of the trans-Niño SST pattern (i.e., east–west

[4] Examining the weaker and/or lack of tropical Pacific SST correlations in the earlier epoch is thus not insightful in this regard.

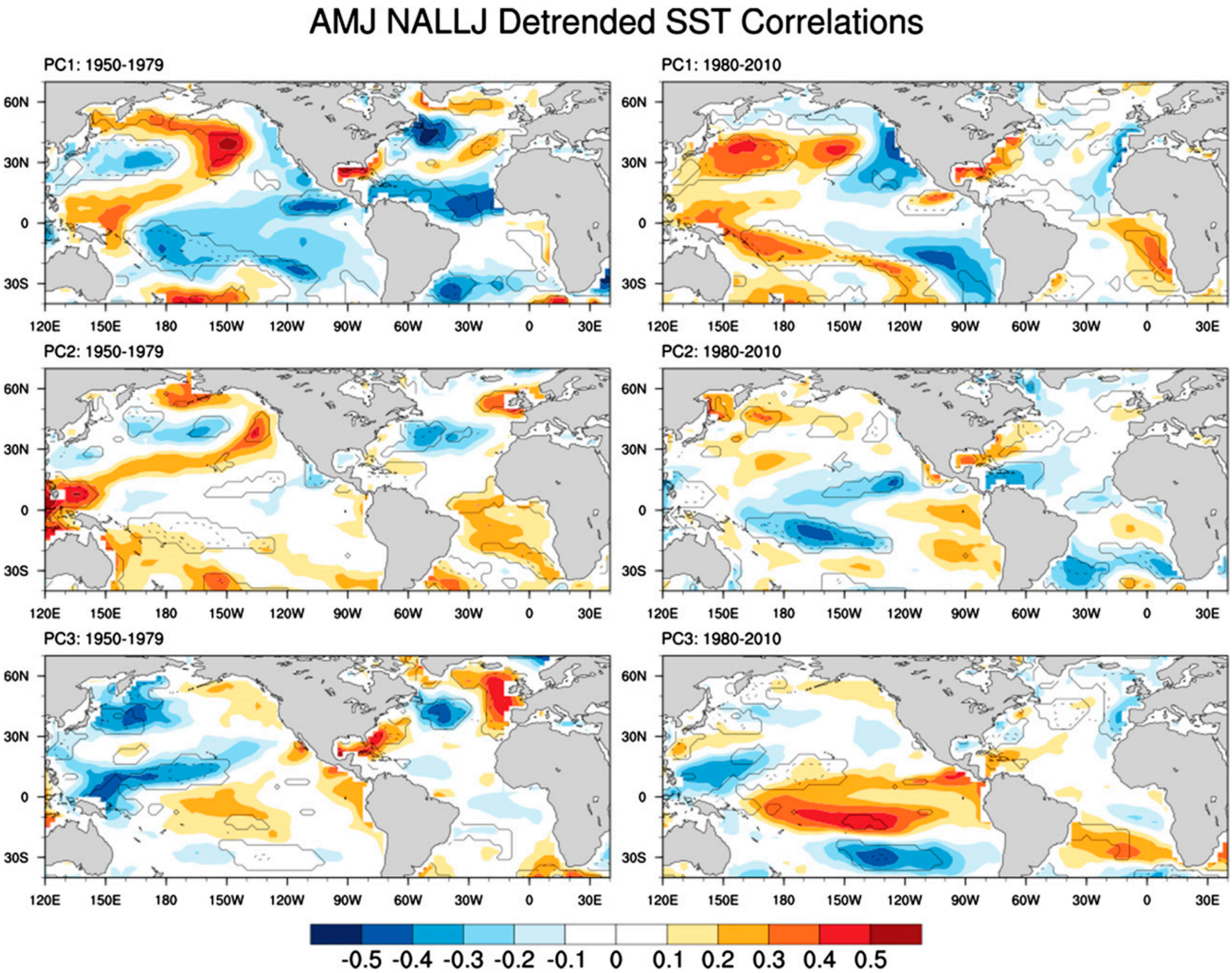

FIG. 6. Correlations of NALLJ modes to SST for (left) 1950–79 and (right) 1980–2010 for (top) PC1, (middle) PC2, and (bottom) PC3. Correlations are shaded at 0.1 intervals and the statistical significance of the correlation difference between the 1950–79 and 1980–2010 periods are contoured at the 70% (solid) and 90% (dashed) levels.

SST gradient). This ENSO-transitioning SST pattern has been linked to the enhancement of low-level moisture flux into the SE region and resultant increases in severe weather outbreaks on seasonal time scales (Lee et al. 2013; Weaver et al. 2012) and is seen here directly in relation to NALLJ mode 2. NALLJ mode 3 (Fig. 8) lag–lead SST regressions exhibit similarities to mode 2 with regard to the seasonal evolution of the related SST structure (i.e., preceding fall–winter maxima and subsequent decay); however, the mode 3 warm SST regressions are much stronger in all seasons and shifted toward the eastern Pacific when compared to that of mode 2.

b. Atmospheric circulation

It is tempting to attribute the significantly weaker contemporaneous (i.e., AMJ) SST connectivity when compared to prior seasons as signifying a diminished role for tropically induced impacts on the large-scale atmospheric circulation, and its potential modulation of NALLJ variability during spring. However, numerous observational and modeling studies show a significant atmospheric response over the tropics at a 1–2 season lag from the wintertime maximum in SST anomalies associated with ENSO, despite the quickly weakening tropical SST anomalies. This evidently occurs as the result of two possible mechanisms. One is due to the delayed response in tropical precipitation (and thus atmospheric diabatic heating profiles) to the maximum in total SST, as the result of the phase interaction between the SST anomaly and the seasonal cycle, which despite the weakening SST anomaly, maximizes during spring [Kumar and Hoerling (2003) and references therein]. The other mechanism is dependent upon how the winter ENSO phase transitions into AMJ. Modeling studies have shown that an

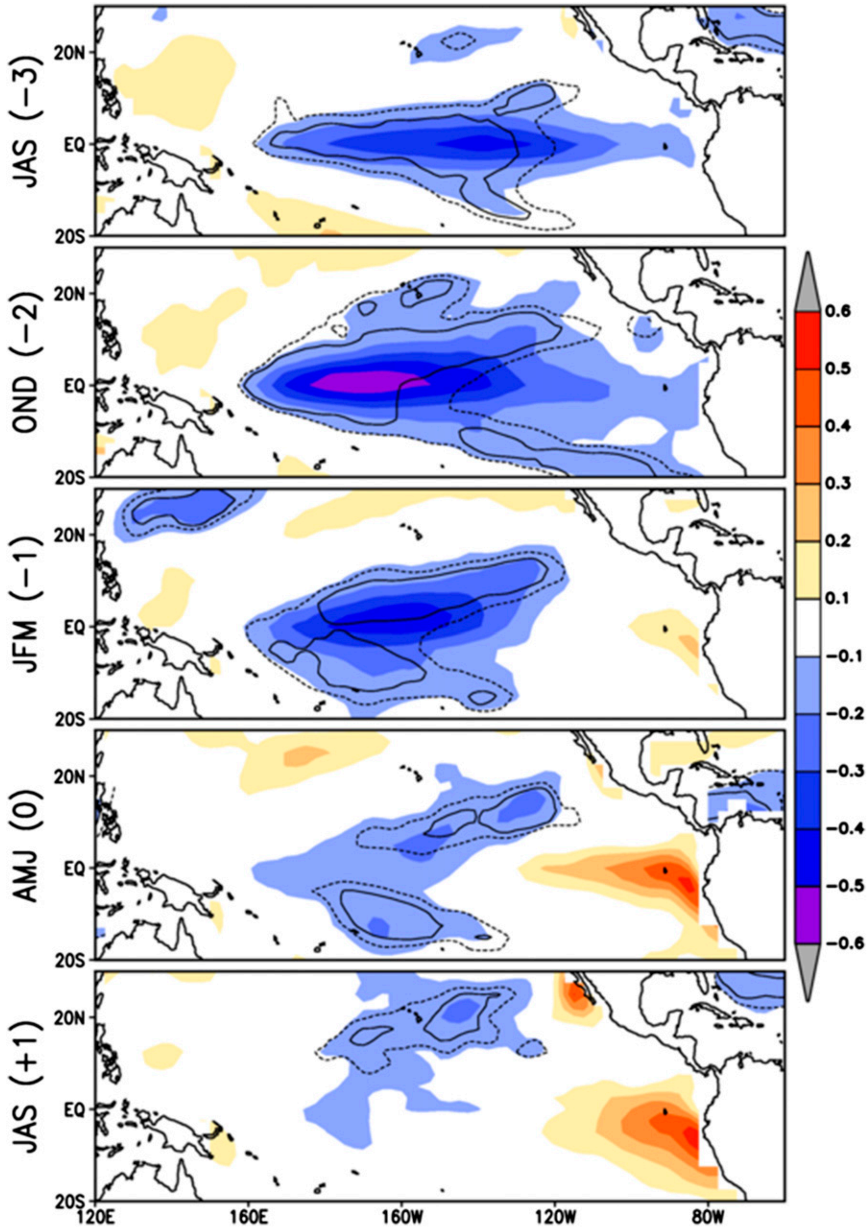

FIG. 7. (top)–(bottom) Five-season lag–lead (from −3 to +1 seasons) regressions of NALLJ PC2 on seasonal SST anomalies (K) centered on AMJ ($t = 0$) for 1980–2010. The 95% (90%) significance according to a t test is contoured with a solid (dashed) line.

oppositely signed SST anomaly between the eastern and central tropical Pacific (i.e., east–west SST gradient as captured by the trans-Niño index) forces a PNA-like upper-tropospheric response over North America (Lee et al. 2013).

Figure 9 shows the large-scale circulation context over the Pacific and North American region and the nature of potential tropical forcing mechanisms as diagnosed via NALLJ PC regressions and correlations for 1980–2010. The 200-hPa geopotential height (z200) correlations (top panel) show a broad tropical-wide negative z200 anomaly with a tripole pattern across the Gulf of Alaska, central Canada, and the southeastern United States, and are reminiscent of the Pacific–North American (PNA) teleconnection pattern. This pattern sets up a strong pressure gradient across the United States that evidently enhances low-level southerly flow and related precipitation anomalies over the southeastern United

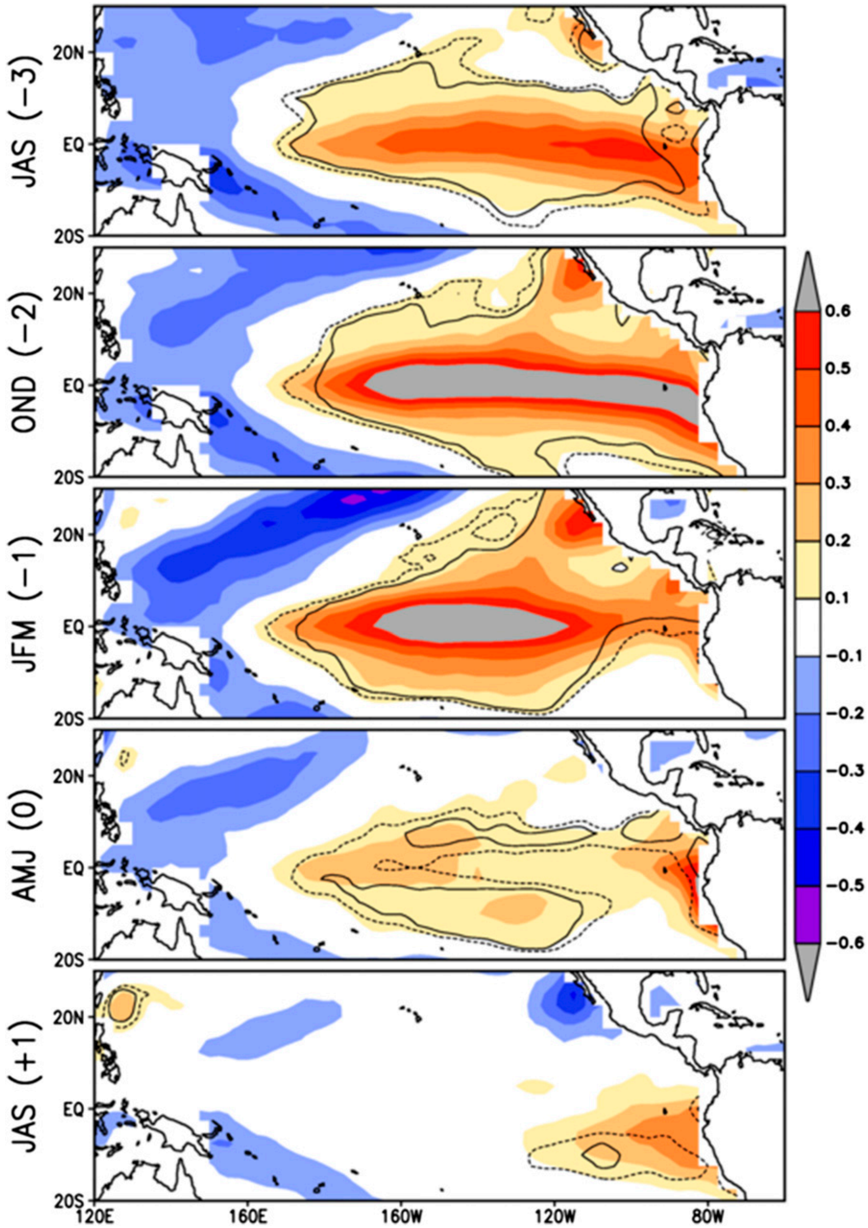

FIG. 8. As in Fig. 7, but for regressions of NALLJ PC3.

States. The question arises as to whether this PNA-like pattern associated with NALLJ mode 2 is tropically forced during AMJ in the midst of a decaying La Niña tropical Pacific SST pattern. While forcing attribution is difficult to discern observationally, examining anomalies of tropical heating, upper-level divergent outflows, and wave emanation regions may provide some insight in this regard.

Although tropical heating from SST-induced precipitation anomalies are widely viewed as generating significant global climate anomalies, the underlying circulation teleconnections are dynamically instigated via the RWS from adjacent subtropical regions, as opposed to directly from regions of deep tropical outflow (Sardeshmukh and Hoskins 1988). Given the meridional extent of tropical divergent outflows, the RWS can be large thousands of kilometers poleward of an equatorial diabatic heating anomaly.

The middle and bottom panels of Fig. 9 show the AMJ seasonal anomalies of the RWS and OLR (middle panel), and 200-hPa divergent outflow (bottom panel) regressed against the NALLJ PC2 index. Negative OLR anomalies

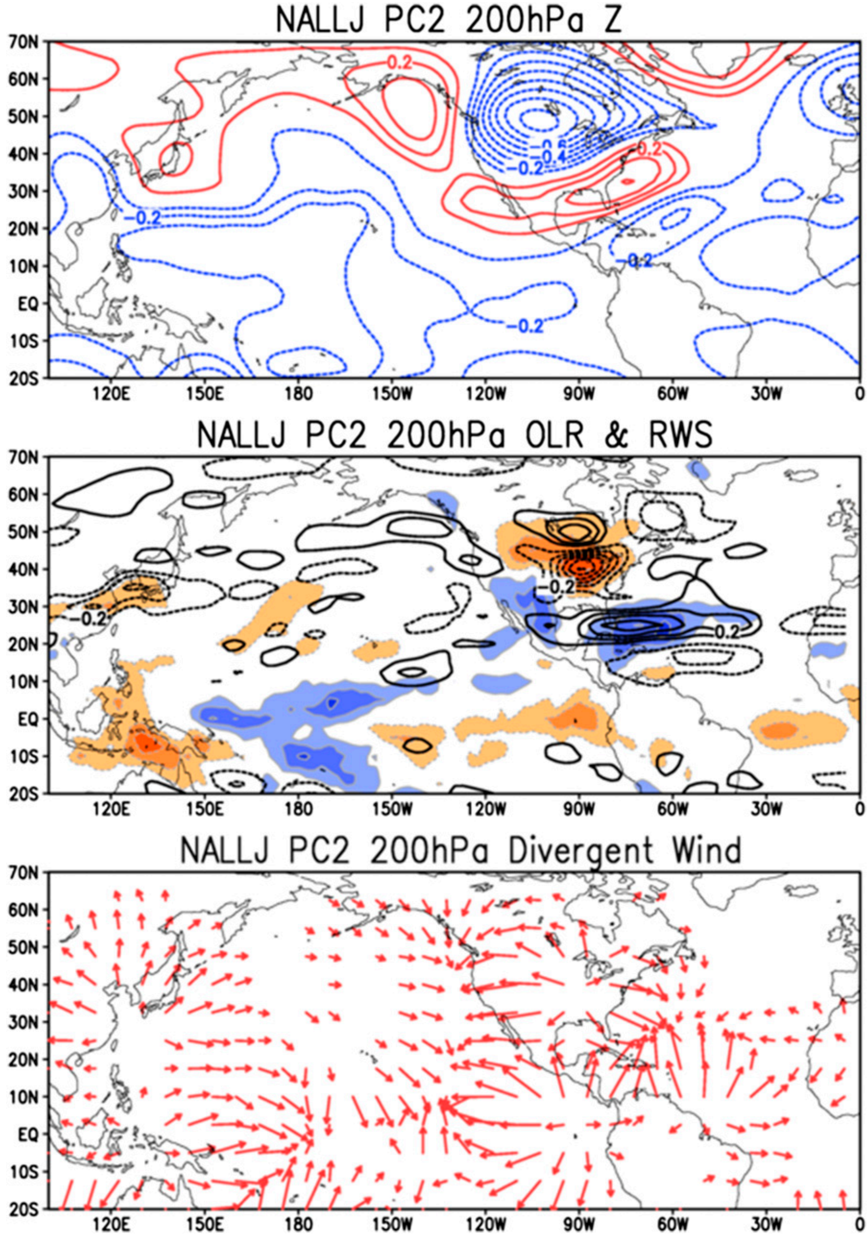

FIG. 9. NALLJ PC2 correlations to (top) AMJ 200-hPa geopotential height, (middle) regressions to OLR and the RWS, and (bottom) the 200-hPa divergent wind for 1980–2010. The 200-hPa correlations are contoured at 0.1 intervals, and regressions of OLR are shaded at $2\,\mathrm{W\,m^{-2}}$ and of RWS are contoured at $1\,\mathrm{s^{-1}}$ (1×10^{10}) intervals. Orange (blue) shading indicates areas of negative (positive) OLR.

(i.e., heating) are present in the far eastern and western Pacific, while positive OLR anomalies (i.e., cooling) are found over the central Pacific. Not surprisingly, these OLR anomalies coincide with the AMJ SST pattern (Fig. 7). Despite the presence of weak RWS regressions (contoured) it cannot be clearly discerned from this analysis if the RWS over the North Pacific region is contributing to the PNA-like teleconnection pattern. Perhaps more striking is the strong RWS regressions over the United States and western Atlantic sector, although this may be part of the quasigeostrophic response itself and may not be necessarily insightful about the wave emanation regions.

Nevertheless, there are two tropical Pacific outflow regions (Fig. 9, bottom) coincident with the negative OLR anomalies in the far eastern and western tropical

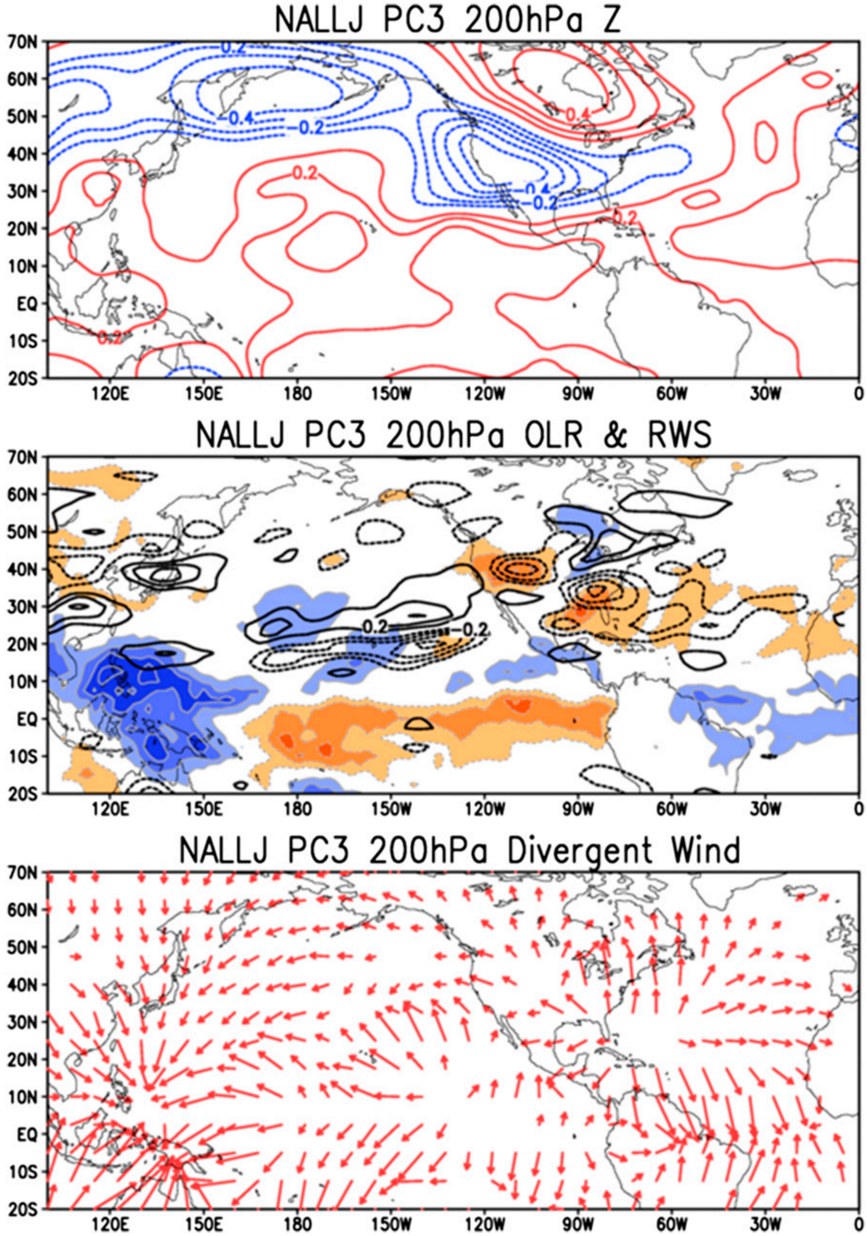

FIG. 10. As in Fig. 9, but for NALLJ PC3.

Pacific. Given the collocation of z200 anomalies over eastern Asia, the RWS anomaly, and the broad area of upper-level divergent outflow, it is possible that this area may be contributing to the generation and/or maintenance of the upper-level height pattern of consequence to NALLJ mode 2. Additionally, the more robust tropical outflow region in the eastern Pacific may also be important for the generation of NALLJ mode 2. The tropical eastern Pacific and eastern U.S. upper-level divergence patterns provide an area of strong upper-level convergence over the Western Hemisphere warm pool region. This is consistent with a positive sea level pressure anomaly over that region (not shown) that has been dynamically linked to enhanced low-level jet activity over the United States (Weaver and Nigam 2008; Wang et al. 2008; Weaver et al. 2009). Despite these intriguing notions, given these varied mechanisms of influence on NALLJ mode 2, and their potential interference, it is not possible to fully attribute their individual contributions without the use of targeted climate model experiments, which are outside the scope of this investigation.

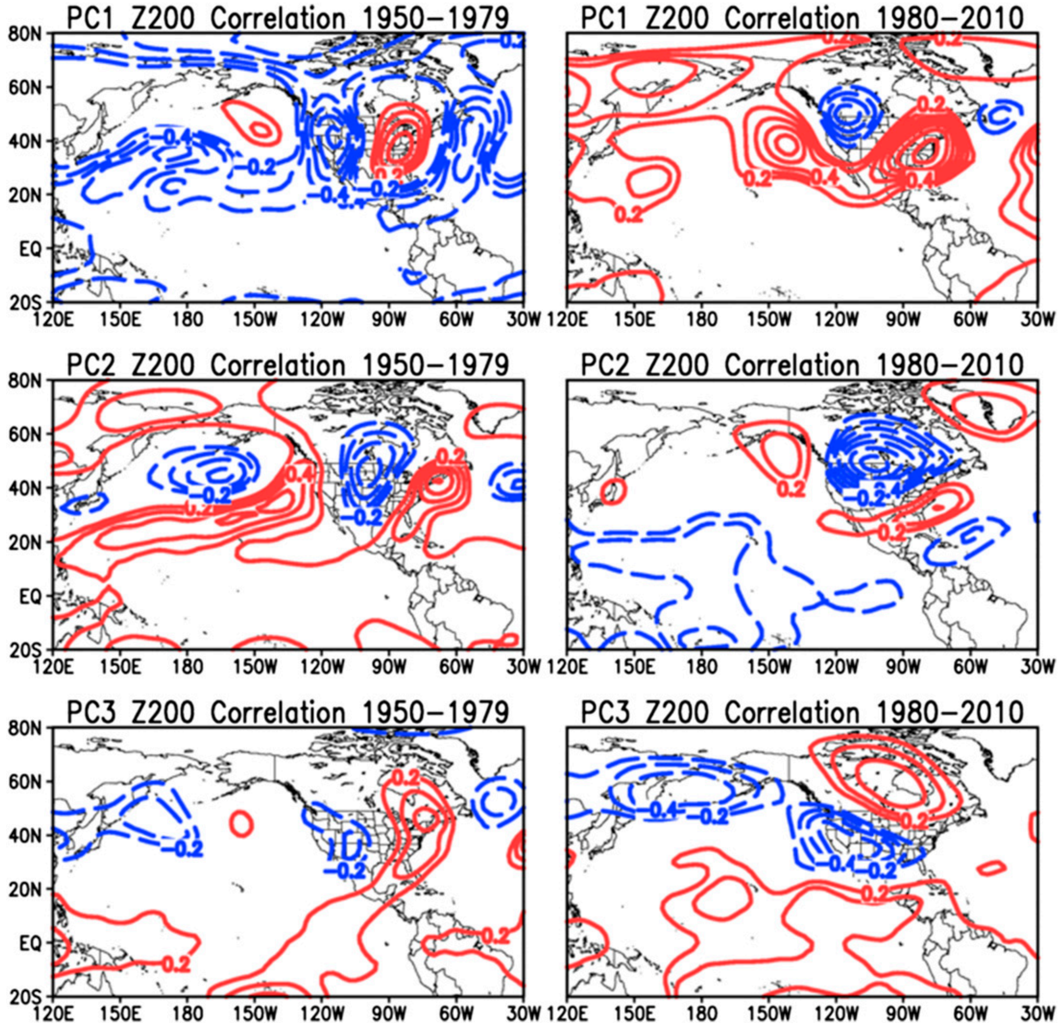

FIG. 11. AMJ correlations of NALLJ PCs on 200-hPa geopotential height anomalies for (top) NALLJ PC1, (middle) PC2, and (bottom) PC3 and for (left) 1950–79 and (right) 1980–2010. Positive (negative) correlations are indicated by solid red (dashed blue) contours.

Figure 10 similarly shows the large-scale circulation context for NALLJ mode 3. Positive 200z spans a large area of the tropical and subtropical regions across the Pacific and Atlantic with strong negative height anomalies over the high-latitude Pacific and much of the United States. The OLR, RWS, and divergent outflow anomalies in the Pacific are much stronger and more coherent than that of NALLJ mode 2, suggesting a more robust role for tropically induced teleconnections in generating the large-scale circulation environment in which NALLJ mode 3 is embedded.

6. Discussion

Recent studies indicate that interannual variability of summertime (i.e., JJA) precipitation has intensified over the southeastern United States during the last six decades (Wang et al. 2009, 2010; Li et al. 2011). Upon closer examination it is evident that changes in this variability are more nuanced and expansive than previously thought. During spring the NGP, SGP, and SE all show an intensification of interannual variability of precipitation during 1950–2010.

Changes to NALLJ variability, characterized by southward and/or eastward shifts in meridional winds in the recent 30 years when compared to the earlier three decades, reveal that the primary modes of NALLJ variability are related to the continual intensification of AMJ precipitation variability over the NGP and SE during the last 60 years. NALLJ precipitation reconstructions highlight this connection by exhibiting similar changes in interannual variability, and are especially noteworthy

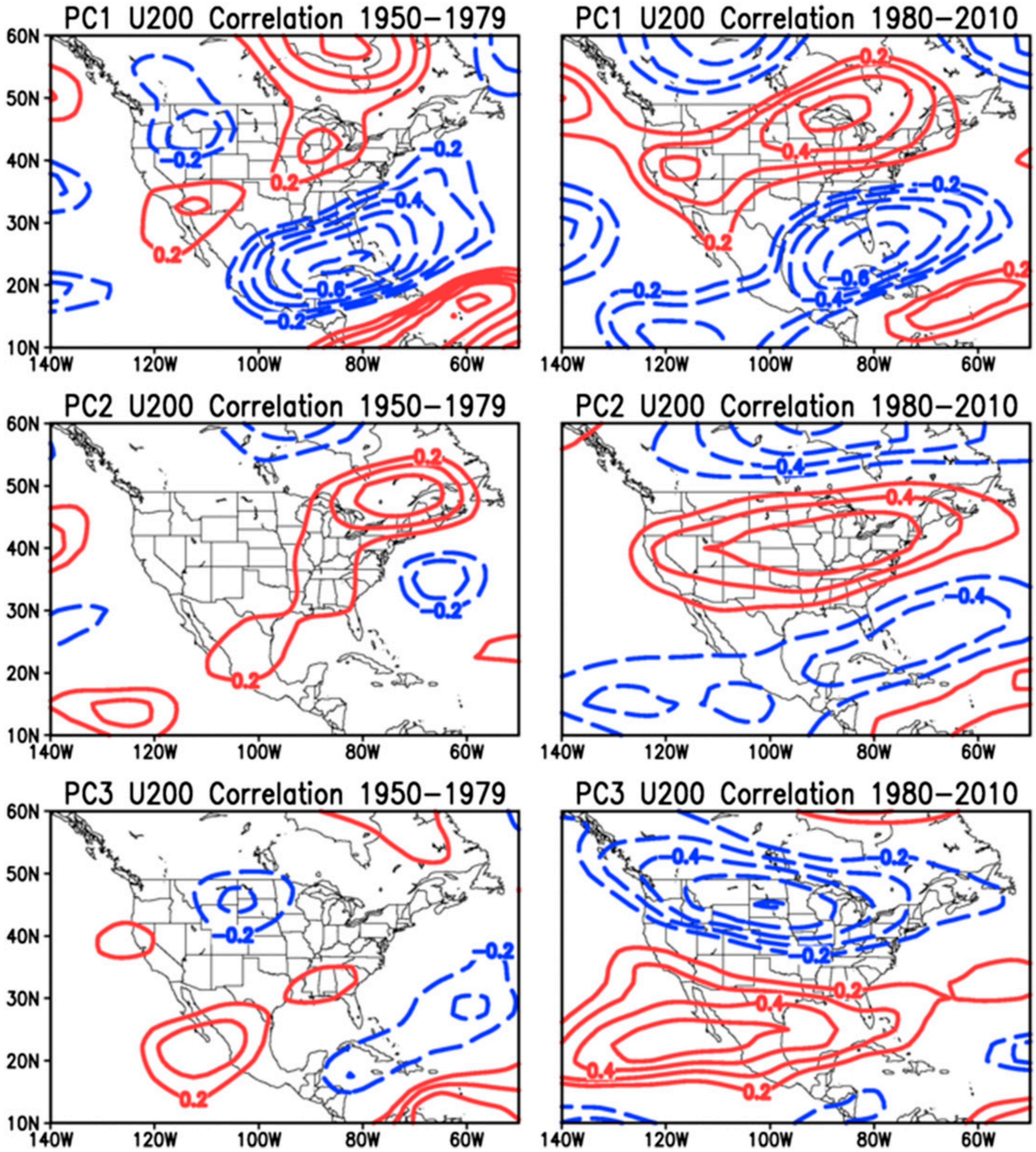

FIG. 12. As in Fig. 11, but for zonal wind anomalies.

over the SE during AMJ. While changes in NALLJ variability cannot fully account for the totality of all regional precipitation variability changes (especially over the SGP), they nonetheless are indicative of its vital importance to changes in the precipitation variability over the NGP and SE.

In the context of the first three NALLJ variability modes and their recent changes, it appears that the role of decadal SST variations (NALLJ mode 1) and the emergence of tropical Pacific connectivity via SST-induced atmospheric circulation changes may act to spatially shift the NALLJ variability modes (i.e., meridional winds shift southward and/or eastward enhancing the precipitation variability) in the recent epoch by modulating the large-scale atmospheric circulation.

These epochal shifts are examined in Fig. 11 via changes in the z200 correlations as a function of epoch. During the early epoch (left panels) there is a noticeable lack of z200 correlation for all modes over most of the tropical Pacific, save weak correlations for mode 3. However, there are strong z200 height correlations over much of the Pacific–North American region, especially in modes 1 and 2. Perhaps most revealing is the fact that the z200 height correlations are significantly lacking in meridional gradients over North America during the early epoch. The zonally oriented height gradient is consistent with a weak positive 200-hPa zonal jet structure as shown in Fig. 12 (left panels). Strong (weak) positive upper-level zonal wind anomalies are related to stronger (weaker) southerly NALLJs as the result of direct and indirect circulations into the exit and entrance regions of upper-level zonal jet streaks, respectively (Uccellini and Johnson 1979). The z200 height correlations during the recent epoch include the emergence of connectivity to the tropical Pacific, as seen in SST, and enhanced positive meridional gradients in all three modes—a situation that induces spatial shifts and strengthening in positive upper-level zonal winds (Fig. 12, right) and concomitant shifts and/or strengthening in the NALLJ variability modes during this time period (Fig. 5).

One obvious result of comparing the large-scale atmospheric circulation during two epochs (Figs. 11 and 12) is that, despite the lack of a tropical SST link in the early epoch, significant NALLJ variability exists. This is likely the result of midlatitude forcing internal to the climate system and suggests that there are interdecadal changes in the NALLJ–tropical Pacific SST correlation. In epochs when the connection is manifest, the result is spatial shifting and/or strengthening of the low-level meridional winds (and thus moisture transports into the United States) leading to enhanced regional precipitation variability, on account of the enhanced upper-level meridional height gradients (Fig. 11), which induce stronger upper-level zonal wind anomalies (Fig. 12).

Despite the potential for interdecadal changes in the SST–NALLJ correlation, the origin of the apparent emergence of tropical Pacific SST linkages to NALLJ variability in recent decades is elusive, observationally. While it may be tempting to indulge in a potential role for anthropogenic climate change on the intensification of NALLJ-induced changes in precipitation variability, the observationally based analysis strategy employed here is not sufficient to answer this question. In fact, it can be proffered that the weak upper-level meridional height gradients (Fig. 11, left panels) and resultant weakened upper-level westerly zonal jet anomalies (Fig. 12, left panels) related to all three NALLJ modes in the earlier epoch argues against an anthropogenic influence, given that one potential impact of global warming is to reduce the equator-to-pole temperature gradients and thus weaken upper-level zonal wind anomalies in the midlatitudes. In this scenario the height correlation patterns in each of the recent two 30-yr epochs are expected to oppose those shown in Fig. 11 (i.e., weaker upper-level meridional gradients in the recent epoch), especially since the strongest global warming has occurred over the last 30 years (IPCC 2013).

An alternative argument is that this type of response may have already been under way during the early epoch and has simply been interrupted and/or overwhelmed by more recent natural variability internal to the climate system. In this scenario a return to a situation more closely resembling the earlier epoch is likely and springtime NALLJ-related precipitation variability would begin to decrease. Questions such as these are the focus of ongoing work, which is predicated on climate model simulations to understand the relative roles of natural climate variability and anthropogenic global warming on the changes in interannual variability of warm season precipitation.

Acknowledgments. The authors wish to acknowledge the contributions of two anonymous reviewers whose suggestions greatly enhanced the quality of the manuscript, and the support of the NOAA Modeling, Analysis, Predictions, and Projections (MAPP) Program.

REFERENCES

Brooks, H. E., G. W. Carbin, and P. T. Marsh, 2014: Increased variability of tornado occurrence in the United States. *Science*, **346**, 349–352, doi:10.1126/science.1257460.

Chen, M. P., P. Xie, J. E. Janowiak, and P. A. Arkin, 2002: Global land precipitation: A 50-yr monthly analysis based on gauge observations. *J. Hydrometeor.*, **3**, 249–266, doi:10.1175/1525-7541(2002)003<0249:GLPAYM>2.0.CO;2.

Guo, Z., and P. Dirmeyer, 2013: Interannual variability of land–atmosphere coupling strength. *J. Hydrometeor.*, **14**, 1636–1646, doi:10.1175/JHM-D-12-0171.1.

Higgins, R. W., E. S. Yarosh, J. E. Janowiak, and K. C. Mo, 1997: Influence of the Great Plains low-level jet on summertime precipitation and moisture transport over the central United States. *J. Climate*, **10**, 481–507, doi:10.1175/1520-0442(1997)010<0481:IOTGPL>2.0.CO;2.

IPCC, 2013: Summary for policymakers. *Climate Change 2013: The Physical Science Basis*, T. F. Stocker et al., Eds., Cambridge University Press, 1–29.

Kalnay, E., and Coauthors, 1996: The NCEP/NCAR 40-Year Reanalysis Project. *Bull. Amer. Meteor. Soc.*, **77**, 437–471, doi:10.1175/1520-0477(1996)077<0437:TNYRP>2.0.CO;2.

Kumar, A., and M. Hoerling, 2003: The nature and causes for the delayed atmospheric response to El Niño. *J. Climate*, **16**, 1391–1403, doi:10.1175/1520-0442-16.9.1391.

Lee, S.-K., R. Atlas, D. B. Enfield, C. Wang, and H. Liu, 2013: Is there an optimal ENSO pattern that enhances large-scale atmospheric processes conducive to tornado outbreaks in the United States? *J. Climate*, **26**, 1626–1642, doi:10.1175/JCLI-D-12-00128.1.

——, B. E. Mapes, C. Wang, D. B. Enfield, and S. J. Weaver, 2014: Springtime ENSO phase evolution and its relation to rainfall in the continental U.S. *Geophys. Res. Lett.*, **41**, 1673–1680, doi:10.1002/2013GL059137.

Li, W., L. Li, R. Fu, Y. Deng, and H. Wang, 2011: Changes to the North Atlantic subtropical high and its role in the intensification of summer rainfall variability in the southeastern United States. *J. Climate*, **24**, 1499–1506, doi:10.1175/2010JCLI3829.1.

Liebmann, B., and C. A. Smith, 1996: Description of a complete (interpolated) outgoing longwave radiation dataset. *Bull. Amer. Meteor. Soc.*, **77**, 1275–1277.

Livezey, R. E., and W. Y. Chen, 1983: Statistical field significance and its determination by Monte Carlo techniques. *Mon. Wea. Rev.*, **111**, 46–59, doi:10.1175/1520-0493(1983)111<0046:SFSAID>2.0.CO;2.

Ruiz-Barradas, A., and S. Nigam, 2005: Warm season rainfall variability over the U.S. Great Plains in observations, NCEP and ERA-40 reanalyses, and NCAR and NASA atmospheric model simulations. *J. Climate*, **18**, 1808–1830, doi:10.1175/JCLI3343.1.

Sardeshmukh, P. D., and B. J. Hoskins, 1988: The generation of global rotational flow by steady idealized tropical divergence. *J. Atmos. Sci.*, **45**, 1228–1251, doi:10.1175/1520-0469(1988)045<1228:TGOGRF>2.0.CO;2.

Schubert, S., H. M. Helfand, C.-Y. Wu, and W. Min, 1998: Subseasonal variations in warm-season moisture transport and precipitation over the central and eastern United States. *J. Climate*, **11**, 2530–2555, doi:10.1175/1520-0442(1998)011<2530:SVIWSM>2.0.CO;2.

Smith, T. M., R. W. Reynolds, T. C. Peterson, and J. Lawrimore, 2008: Improvements to NOAA's historical merged land–ocean surface temperature analysis. *J. Climate*, **21**, 2283–2296, doi:10.1175/2007JCLI2100.1.

Uccellini, L. W., and D. R. Johnson, 1979: The coupling of upper and lower tropospheric jet streaks and implications for the development of severe convective storms. *Mon. Wea. Rev.*, **107**, 682–703, doi:10.1175/1520-0493(1979)107<0682:TCOUAL>2.0.CO;2.

Wang, C., S.-K. Lee, and D. B. Enfield, 2008: Climate response to anomalously large and small Atlantic warm pools during summer. *J. Climate*, **21**, 2437–2450, doi:10.1175/2007JCLI2029.1.

Wang, H., S. Schubert, M. Suarez, J. Chen, M. Hoerling, A. Kumar, and P. Pegion, 2009: Attribution of the seasonality and regionality in climate trends over the United States during 1950–2000. *J. Climate*, **22**, 2571–2590, doi:10.1175/2008JCLI2359.1.

——, R. Fu, A. Kumar, and W. Li, 2010: Intensification of summer rainfall variability in the southeastern United States during recent decades. *J. Hydrometeor.*, **11**, 1007–1018, doi:10.1175/2010JHM1229.1.

Weaver, S. J., 2013: Factors associated with decadal variability in Great Plains summertime surface temperatures. *J. Climate*, **26**, 343–350, doi:10.1175/JCLI-D-11-00713.1.

——, and S. Nigam, 2008: Variability of the Great Plains low-level jet: Large-scale circulation context and hydroclimate impacts. *J. Climate*, **21**, 1532–1551, doi:10.1175/2007JCLI1586.1.

——, S. Schubert, and H. Wang, 2009: Warm season variations in the low-level circulation and precipitation over the central United States in observations, AMIP simulations, and idealized SST experiments. *J. Climate*, **22**, 5401–5420, doi:10.1175/2009JCLI2984.1.

——, S. Baxter, and A. Kumar, 2012: Climatic role of North American low-level jets on regional U.S. tornado activity. *J. Climate*, **25**, 6666–6683, doi:10.1175/JCLI-D-11-00568.1.